Performance of PT/CRSE Schottky diodes designed for 5G/6G technology applications

L. H. Kh. Alfhaid[a], A. F. Qasrawi[b,c,*]
[a]*Department of Physics, Collage of Science, University of Ha'il, Ha'il, Saudi Arabia*
[b]*Department of Physics, Arab American University, Jenin, Palestine*
[c]*Department of Electrical and Electronics Engineering, Istinye University, 34010, Istanbul, Turkey*

Herein thin films of CrSe deposited by the thermal evaporation technique onto Pt substrates are designed as Schottky diodes. It is observed that the Pt/CrSe/C (PCC) Schottky diodes are of tunneling type showing barrier height and widths of 0.56 eV and 18 nm, respectively. These diodes displayed biasing dependent nonlinearity and negative slope of differential resistance. The analyses of the cutoff frequency spectra indicated that PCC devices can exhibit high cutoff frequency up to 17 GHz based on the driving signal frequency. The features of the PCC devices make it promising as electronic component suitable for 5G/6G technology applications.

(Received October 27, 2023; Accepted January 11, 2024)

Keywords: Pt/CrSe, Tunneling barriers, Microwaves, Cutoff frequency, 6G technology

1. Introduction

Chromium based materials has attracted the focus of researchers due to their novel applications. They are regarded as one of the hardest transitions metal compounds and appears a promising material for the superconducting technological applications [1, 2]. Chromium based materials is also featured for nanoelectronics and clean energy harvesting [3]. As for examples Janus Cr_2NY (Y=P, As, Sb) compounds displayed great potential for various applications [3]. They performed as active materials for electrocatalytic hydrogen-evolution and as spin gapless semiconductor (Cr_2NSb) [3]. $CrPS_4$ is also employed as a semiconducting layer in the fabrication of spin-field effect transistors [4].

One of the promising chromium based compounds that captured the interest is chromium selenide. This compound can exist in different polymorphic phases including $CrSe_2$, Cr_2Se_3, Cr_7Se_8 and CrSe [5]. Each of these phases' exhibited different crystal structure and different thermal, electrical, magnetic and optical properties [5]. This property made the material under focus attractive for various applications. As for examples Cr_2Se_3 showed novel thermoelectric properties that make it compatible with commercial thermoelectric materials [5]. On the other hand $CrSe_2$ polymorphic phase of chromium selenide is a magnetic material exhibiting large tunneling magnetoresistance which make it ideal for fabrication of magnetic tunnel junctions [6]. Due to the scalability, low power consumption and nonvolatility these magnetic junction finds spintronic applications [6].

Although literature data reported many applications for chromium selenide thin films. Applications of this material in gigahertz technology are rarely reported or almost absent. For this reason here in this work we are motivated to fabricate n- types chromium selenide Schottky barriers that can be used in 5G/6G communication technology as antennas or microwave signal receivers. The work here will include identification of the work function of CrSe which is a key parameter for determining the nature of metal contacts (Ohmic/Schottky). The work function will be determined with the help of the optical and temperature dependent electrical resistivity measurements. In addition, the role of platinum as a Schottky contacts on the growth nature, atomic stoichiometry and electrical performance will be considered. Platinum was selected

* Corresponding author: atef.qasrawi@aaup.edu
https://doi.org/10.15251/JOR.2024.201.65

because it has higher work function than that of CrSe. Platinum is also preferred because of its relatively high stability and catalytic efficiency. Pt can easily form Pt-Se bonds which reduces the number of broken bonds in CrSe [7]. This results in less defective interfaces. Pt proofed its effective performance as substrates for gigahertz terahertz technology applications [8]. While the surface morphology and structural modifications are explored by the scanning electron microscopy and X-ray diffraction techniques, the electrical performance as gigahertz filters will be determined by the current-voltage and impedance spectroscopy techniques. Some theoretical models which target at exploring the limits of the Pt/CrSe as 5G/6G communication technology tool will be employed.

2. Experimental details

The fabrication of the gigahertz devices is initiated by depositing thin films of platinum onto ultrasonically cleaned glass substrates in a vacuum media. For this purpose an ion coater was employed. High purity platinum sputtering targets (99.99%, Alpha Aeser) was used. Pt thin film substrates of thicknesses of 300 nm were coated. The produced Pt substrates were loaded into a NORM-600 thermal evaporator and located 22 cm above the evaporation source. The evaporation source was chromium selenide powders (99.9%, Apha Aeser) filled in a boat shaped tungsten heater. The system was evacuated to 10^{-5} mbar before the evaporation cycle started. Some of the CrSe films were deposited onto glass to allow optical measurements. Others which are also coated onto glass were of Hall bar shape to allow electrical resistivity measurements. The evaporation of chromium selenide thin films was carried out at a growth rate of 7 nm/s. Films of thicknesses of 500 nm were obtained. The films were structurally characterized using the X-ray diffraction unit (Miniflex 600). The energy dispersive X-ray spectroscopy attached to a COXEM-200 scanning electron microscope was measured using EDAX type detectors. The conductivity type was determined using the hot probe technique. CrSe thin films coated onto glass exhibited n-type conductivity. Optical measurements were handled in the spectral range of 300-1100 nm using Thermoscientific Evolution 300 spectrophotometer. Electrical resistivity measurements were actualized in an ARS closed cycle He-cryostat. The current (I)-voltage (V) characteristics was collected with the help of Keithley I-V system composed of Keithley 2481 picoammeter and Keithley 231 voltage source. The impedance spectroscopy was measured using Agilent4291B 0.01-1.80 GHz impedance analyzer.

3. Results and discussion

The schematics for the Pt/CrSe/C Schottky diode are shown in the inset of Fig.1 (a). The X-ray diffraction measurements on these diodes displayed no sharp patterns indicating the disordered nature of growth of CrSe onto glass or Pt thin film substrates. The only sharp patterns are those of Pt substrates (JCPDS PDF card No. 040802). Deeps scanning electron microscopy (SEM) analyses on these thin films which are illustrated in Fig. 2 (b) and (c) indicated the formation of grains of average sizes of 220 nm for films deposited onto glass substrates. SEM images for films deposited onto Pt substrates are illustrated in Fig. 2 (c). The nature of grain growth here is very different displaying very dense spherical grain distribution. The average sizes of these spherical grains is1.0 μm. Some exceptionally large grains can also be detected in Pt/CrSe films. On the other hand the energy dispersive X-ray (EDS) measurements represented in the inset of Fig. 1 (c) showed the existence of glass ($SiO:Na_2O:MgO:CaO$), Pt, Au, Cr and Se only. No other elements were observed in the spectra. It means that the grown films are of high purity. Here Au existed because it was coated onto the films surfaces to prevent possible electron contaminations during SEM experiments. The numerical data of EDS measurements have shown that both of glass and Pt films did reveal the same atomic contents of CrSe. Particularly, films deposited onto lime glass displayed atomic content of 66.67 at. % Se and 33.33 at. % Cr. Films grown onto Pt substrates displayed atomic contents of 51.87 at. % Se and 48.13 at. % Cr. In other

words films deposited onto glass and Pt substrates prefer $CrSe_{2.00}$ and $CrSe_{1.08}$ forms of chromium selenide.

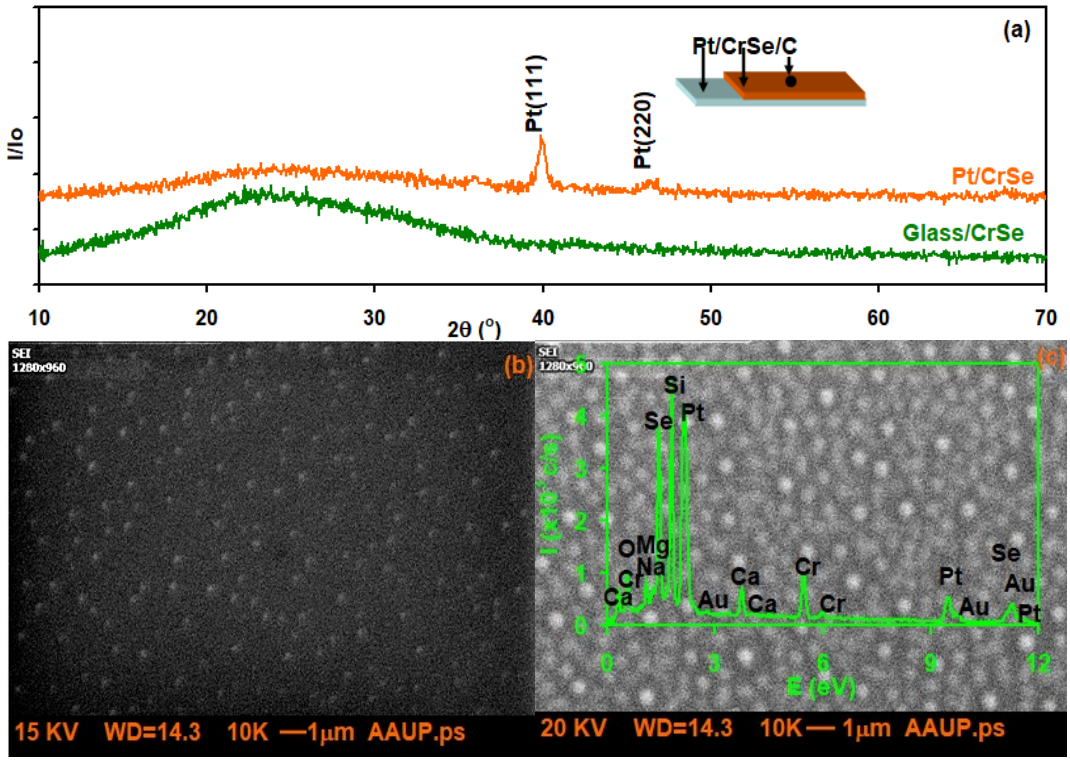

Fig. 1. (a) The X-ray diffraction patterns and the scanning electron microscopy image for (b) glass/$CrSe_2$ and (c) Pt/CrSe films. The inset of (a) showing the schematics for the Pt/CrSe/C devices and inset of (c) showing the energy dispersive X-ray spectra for Pt/CrSe films.

Conversion of $CrSe_2$ to CrSe in the presence of Pt as catalysts can be ascribed to the thermodynamic stability. Actually both of the Pt-Se and Cr-Se bonds exhibit the same bond length (254 pm [7-9]) indicating that they exhibits close values of bonding energy. However because the ionic radius of Pt^{2+} and Pt^{4+} being 80 pm and 62.5 pm [10], respectively are larger than that of Cr^{+4} (41 pm [11]) and smaller than those of Cr^{+2} (85 pm [12]) then the probable occupancy of the Cr^{+2} site by Pt cations become possible. In addition as Pt films are coated before CrSe films some of the unreacted Cr^{+4} atoms have the chance of filling the vacant sites of Pt^{+2} and Pt^{+4}. The repulsive interaction between Cr and Pt leads to the formation of periodically modulated structures [13]. Repulsive interactions also result in degradation of crystalline morphology [14]. By repulsive interactions the kinetic energy of the system increases [15]. It seems that for $CrSe_2$ under conditions where repulsive interactions dominate, thermodynamic stability is achieved by structural transformations and exchanges in bonding mechanisms. The formation of chromium selenide onto Pt slabs should then be accompanied with structural transformations. Indeed, the most famous structural phases of $CrSe_2$ are hexagonal and trigonal corresponding to the point group symmetries D6h and D3d, respectively [16]. The hexagonal phase is more stable than the trigonal phase [16]. On the other hand CrSe phase reaches thermal stability in the space group P4/nmm by featuring a square lattice in the ab-plane. In this process two layers of Cr^{+2} cations are sandwiched between two layer Se^{-2} anions [17]. Hence Pt ionic substitutions which forced charge reduction from Cr^{+4} to Cr^{+2} are associated with structural transitions. The weak crystallinity of the films could account for the failure of the XRD technique to detect sharp patterns relating to these expected structures.

In order to establish a correct energy band diagram for the Pt/CrSe devices, information about the energy band gap value was gained from the optical absorption coefficient and electrical resistivity measurements. The absorption coefficient (α) spectra for glass/$CrSe_2$ films are illustrated in Fig. 2 (a). The spectra show two different decay regions in α −values resulting from decreasing incident photon energy (E). The decrease in α values above 3.83 eV (high decay region (3.83-4.20 eV)) is sharper than the below region (1.17-3.83 eV). Direct allowed transitions energy band gap of 2.60 eV is determined from the fitting of Tauc's equation ($(\alpha E)^2 - E$) which is also illustrated in Fig. 2 (a). Further details about the optical absorption and band transitions in addition to dielectric dispersion can be found elsewhere [19]. In addition the position of Fermi level ($E_F = \frac{E_c - E_d}{2}$, E_c is conduction band minima and E_d is the donor levels in $CrSe_2$ films) is determined from the Arrhenius plot of the electrical resistivity which is displayed in the inset of Fig. 2 (a). In accordance with the relation $= \rho_o e^{\frac{E_d}{kT}}$ [20], the donor level obtained from the slope of the $\ln(\rho)$-$1000/T$ variation is centered at $E_d = 28$ meV. Recalling from literature data that the electron affinity of $CrSe_2$ is 5.05 eV [18] then the work function ($q\phi = q\chi + |E_F - E_c|$) of CrSe is 5.064 eV. Because $CrSe_2$ thin films showed n −type conductivity and because the metal work function of Pt being 5.65 eV [21] is larger than that odf $CrSe_2$ then a Schottky barrier of barrier height ($q\phi_{Pt/CrSe} = |q\phi_{Pt} - q\chi_{CrSe2}|$ [20]) of 0.60 eV is determined. The energy band diagram for the Pt/CrSe devices is established and presented in Fig. 2 (b). One main feature of Schottky barriers is their fast switching speed due to the absence of depletioning region [21]. They also consume less power because they work at low forward biasing voltages [20].

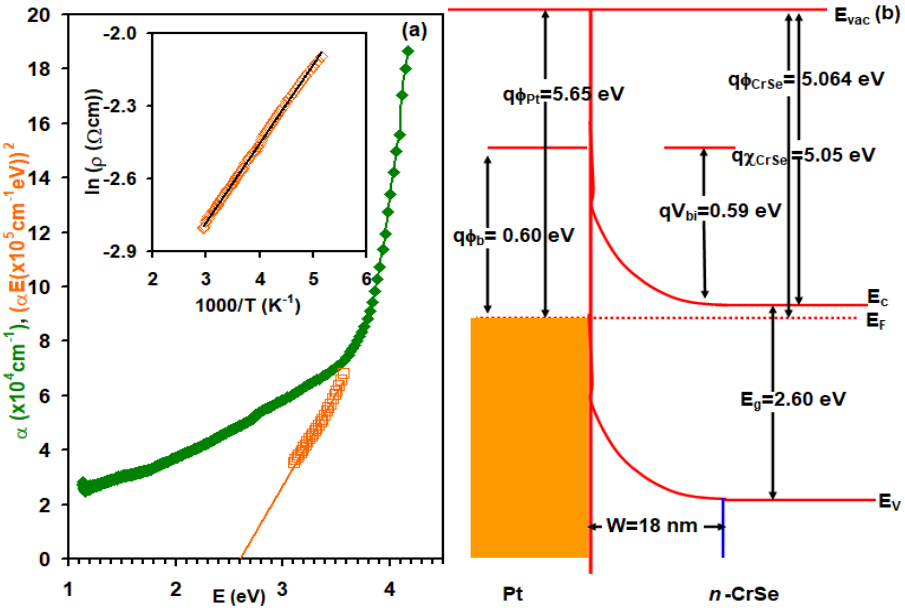

Fig. 2. (a) the absorption coefficient spectra and the Tauc's equation fittings and (b) the energy band diagram for Pt/CrSe Schottky diodes. Inset of (a) showing the Arrhenius plots for electrical resistivity measured for Hall bar type samples of glass/$CrSe_2$ films.

In order to register electrical data from the Pt/CrSe Schottky barriers and avoid formation of back to back (Pt/CrSe/Pt) Schottky barriers carbon ($q\phi_C = 4.65 - 5.1$ eV [22, 23]) is used as an Ohmic contact. The current (I)- voltage (V) characteristics for the Pt/CrSe/C (PCC) devices are presented in Fig. 3 (a). It is clear from the figure that the diodes under study show large reverses currents indicating the tunneling type devices. In these devices large reverse current prevails because the charge carries found a high and narrow barrier forcing current conduction by quantum mechanical tunneling [20]. For these diodes the current is usually dominated by electric

field assisted thermal excitations or simply by tunneling in which the current takes the from [20, 23, 24],

$$I_{QMT} = AA^{*}T^{2}\exp\left(-\frac{e(\phi_b-\sqrt{e/(4\pi\varepsilon_o\varepsilon_r)}\,\sqrt{V}/\sqrt{w})}{kT}\right), \quad (1)$$

In Eqn. (1) the area $A = 0.0314$ cm^2 and Richardson constant A^{*}=120$m^{*} = 36$ A/(cm^{2}K^2) ($m^{*} = 0.30m_o$ [25]). $q\phi_b$ is the biasing independent barrier height. It exhibited value of 0.60 eV in accordance with the energy band diagram presented in Fig. 2 (b). ε_r=5.0 is the high frequency dielectric constant [19] and W is the width of the tunneling barrier. The fitting of Eqn. (1) is presented by solid black circles in Fig. 3 (a). The good fitting of the experimental data was achieved for a barrier height of 0.56 eV and barrier width of 18 nm. The theoretically estimated $q\varphi_b$ value being 0.56 eV is very close to that determined as 0.60 eV from optical and electrical measurements. Such types of tunneling diode are mentioned suitable for the design of long range and low power microwave antennas [26]. They can also be employed as high frequency signal receivers [27].

In cases where PCC diodes are used as antennas two important parameters should be considered. One is the differential resistance (R_D) and the other is the nonlinearity (NL) as a figure of Merit. They are defined as [28],

$$R_D = \left(\frac{dI}{dV}\right)^{-1} \quad (2)$$

$$NL=\frac{dI/dV}{I/V}. \quad (3)$$

The biasing dependence of these two parameters is presented in Fig. 3 (b) and (c), respectively. It is clear from Fig. 3 (b) that the differential resistance decreases with increasing biasing voltage. It decreases from ~600 Ω when the device is unbiased ($V = 0$ .0 V) to ~79 Ω as the diode is reverse biased with $V = 1.0$ V. Forward biasing (V_F) of the device at 1.0 V reveal R_D values of 130 Ω. The slopes of the $R_D - V_F$ dependence are always negative. The negative differential resistance (NRD) is a feature of tunneling diodes (Esaki diodes) operating in the NRD mode [20]. On the other hand the NL-V dependence illustrated in Fig. 3 (c) increase with increasing voltage exceeding values of NL =2.0 at $V = \pm 1.0\,V$. This value of NL indicates remarkable level of nonlinearity which means that small variations in the biasing voltage results in relatively large changes in the current. Such property is crucial for particular applications where precise voltage controlled oscillators and amplifiers are required [20].

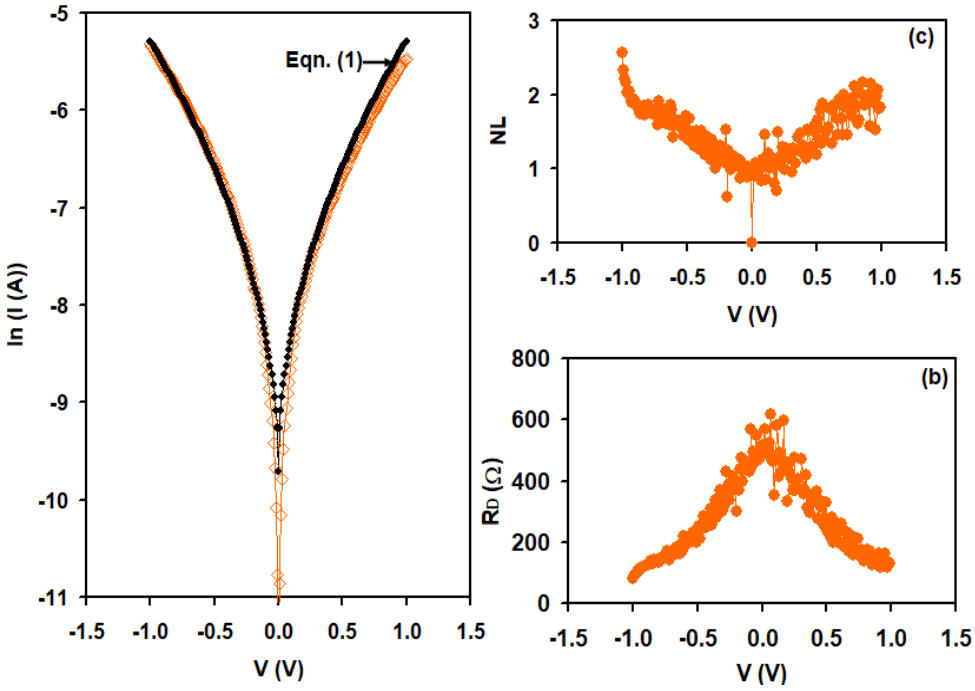

Fig. 3. (a) the current- voltage characteristics, (b) the biasing dependent differential resistance and (c) the biasing dependent nonlinearity of for Pt/CrSe/C tunneling diodes.

Literature data reported values of $R_D = 405\ \Omega$ at $V_F = 0.0\ V$ and decreases to 92 Ω at $V_F = 0.30\ V$ for Pt/HfO_2/Au diodes used as rectennas [28]. The NL values of this device exceed 2.0 at $V = 0.30\ V$ [28]. These devices which operate as a rectifier and as an antenna are used to convert electromagnetic energy in the form of radio and microwaves into direct current [20]. They are of interest of the wireless power transmission technology. As they easily convert signals into electricity [20, 28].

To test the facilities of the PCC devices as signal receivers (or antennas), the device was inserted between the terminals of an impedance analyzer. A signal of low amplitude (less than 0.10 V) and varying driving frequency (f) was imposed between the terminals of the PCC devices. The conductance (G), capacitance (C) and impedance (Z) spectra were recorded in the driving frequency domain of 0.01-1.80 GHz. The conductance spectra are shown in Fig. 4 (a). It increases with increasing signal frequency following a power law of the form $G = 1.24 \times 10^{-3} f^{1.66}$. The conductance increases with increasing frequency under conditions where charge carriers exhibit higher mobility and faster hopping processes [29]. The deviation of the power exponent from 1.0 indicates the possible domination of both of the quantum mechanical tunneling and correlated barrier hopping mechanism at a time in the device under study [30].

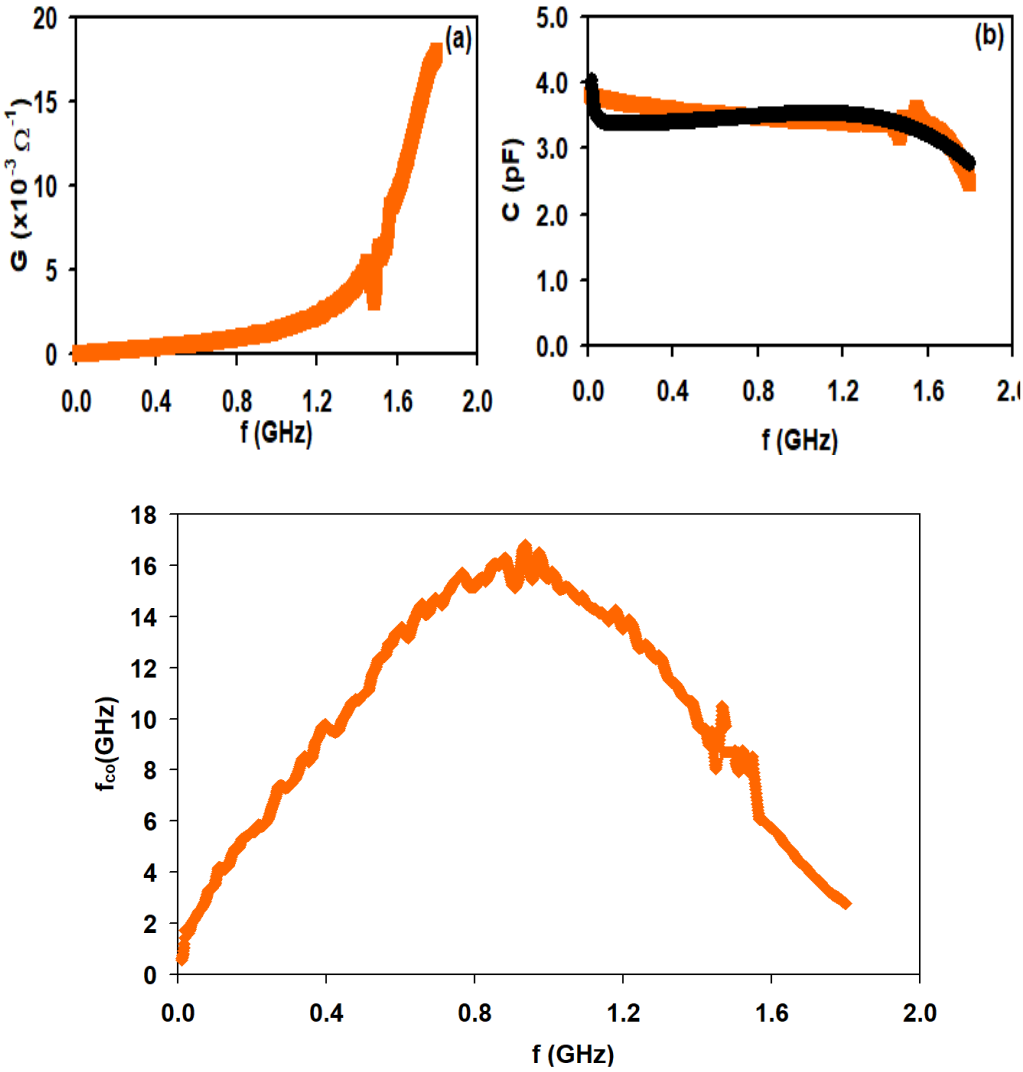

Fig. 4. (a) the conductance, (b) the capacitance and (c) the cutoff frequency spectra for the PCC tunneling diodes.

Fig. 4 (b) show the capacitance spectra for the PCC devices. The capacitance decreases with increasing signal frequency showing a sharper decay as the frequency values exceeds 1.54 GHz. Such behavior provides an evidence about the continuous distribution of interface states [31]. However as the capacitance is directly proportional to the dielectric constant, more accurate information about the behavior of the capacitance spectra is gained from Lorentz approach for dielectric dispersion. In Lorentz oscillator models the dielectric constant takes the form [32],

$$\varepsilon(w) = \varepsilon_\infty + \sum_{i=1}^{N} \frac{n_i e^2}{\varepsilon_o m^*} \frac{w_{oi}^2 - w^2}{(w_{oi}^2 - w^2)^2 + (\gamma_i w)^2}. \quad (4)$$

In the above equation, ε_∞ represents the high frequency dielectric constant, N is the number of possible oscillators, w_o is the oscillator radial frequency, n_i is the free electron concentration associated with the oscillator i, $m^*$is the reduced effective mass for Pt/CrSe system and γ_i is the electronic friction coefficient of damping force and is given as the inverse of the scattering time constant (τ_i) of electrons. For the device under focus $m^* = \left(\frac{1}{m_{Pt}^*} + \frac{1}{m_{crse}^*}\right)^{-1}$ $= \left(\frac{1}{1.0m_o} + \frac{1}{0.30m_o}\right)^{-1} = 0.23m_o$ [25, 34] is substituted in Eqn. (4). In accordance with this model

running the series up to $N = 2$ was sufficient to reproduce the capacitance spectra. The fitting of Eqn. (4) is shown in Fig. 4 (b) by black colored circles. The fitting parameters that reproduced the experimental data are listed in Table-1. The tabulated data indicate the presence of two oscillators one in the radiowave range exhibiting value of 10 MHz and the other in the microwave range exhibiting value of 2.70 GHz. The free electron density of the radiowave oscillator is larger than that of the microwave oscillator. The decrease in the free electron density is accompanied with longer scattering time constant. The increase in the scattering time is assigned to the reduced free electron density. The free electron density decreases due to the inability of the electrons to orient with the varying ac signal at high frequencies [35].

Table 1. Lorentz oscillator parameters for PCC devices.

Parameter	N=1	N=2
C_{core} (pF)	3.8	3.8
w_o (GHz)	0.01	2.7
n ($\times 10^{10}$ cm^{-3})	8.0	4.3
τ (ns)	0.2	0.42

On the other hand for the PCC devices under studying the microwave cutoff frequency ($f_{co} = G/(2\pi C)$ [20]) spectra are shown in Fig. 4 (c). Promising values of f_{co} can be seen from the figure. Particularly The cutoff frequency increases from ~1.0 GHz to ~17 GHz as the signal frequency is tuned in the range of 0.01-0.94 GHz. Larger ac frequency values leads to lower f_{co} values. Literature data reported values of f_{co} larger than 12.0 GHz being adequate for 5G/6G technology needs [34]. A cutoff frequency of 15 GHz is also reported as appropriate value for 5G/6G technology needs [36]. It means that the PCC devices are within the class of devices that can be employed for the 5G/6G communication technology.

4. Conclusions

Here we have fabricated Pt/CrSe Schottky type devices by the ion coating and thermal evaporation techniques. The produced thin films were characterized by structural, compositional, morphological, optical and electrical methods. Having identified the band gap of CrSe as 2.60 eV and the donor level as 28 meV, the work function (5.064 eV) is determined and the barrier height (0.60 eV) of the Pt/CrSe Schottky diodes was identified. The devices were observed to be of tunneling type showing a tunnel diode characteristics with barrier width of 18 nm. From practical point of view Pt/CrSe tunneling diodes performed as negative differential resistance sources with pronounced nonlinearity values. The Pt/CrSe devices were also treated as microwave band filters. They displayed promising cutoff frequency values larger than 17 GHz. The Pt/CrSe device structure is suitable for tunneling based devices and as resonator (filters) for 5G/6G technology needs.

Acknowledgments

This research has been funded by Scientific Research Deanship at University (DSR) of Ha'il Saudi Arabia through project number BA-22028. The authors, therefore, gratefully acknowledge the DSR technical and financial support.

Funding

This research has been funded by Scientific Research Deanship at University of Ha'il Saudi Arabia through project number BA-22028.

References

[1] Kvashnin, Alexander G., Artem R. Oganov, Artem I. Samtsevich, Zahed Allahyari, The journal of physical chemistry letters 8, no. 4 (2017): 755-764; https://doi.org/10.1021/acs.jpclett.6b02821

[2] XU, Hanxiang. Theory for superconductivity and magnetism in layered titanium and chromium based materials. (2023).

[3] Li, Lei, Tao Huang, Kun Liang, Yuan Si, Ji-Chun Lian, Wei-Qing Huang, Wangyu Hu, Gui-Fang Huang, Physical Review Applied 18, no. 1 (2022): 014013; https://doi.org/10.1103/PhysRevApplied.18.014013

[4] Riesner, Maurizio, Rachel Fainblat, Adam K. Budniak, Yaron Amouyal, Efrat Lifshitz, Gerd Bacher, The Journal of Chemical Physics 156, no. 5 (2022); https://doi.org/10.1063/5.0079298

[5] Kariper, I. A., Journal of Non-Oxide Glasses Vol 7, no. 3 (2015): 37-44.

[6] Guo, Xiaoyan, Yu Zhu, Baishun Yang, Xiaolin Zhang, Xiufeng Han, Yu Yan, Applied Physics Letters 121, no. 4 (2022); https://doi.org/10.1063/5.0098687

[7] Zhao, Xu, Ranzhuo Huang, Tianxing Wang, Xianqi Dai, Shuyi Wei, Yaqiang Ma, Physical Chemistry Chemical Physics 22, no. 10 (2020): 5765-5773; https://doi.org/10.1039/C9CP06249A

[8] Alfhaid, Latifah Hamad Khalid, Atef Fayez Qasrawi, Physica Scripta 97, no. 5 (2022): 055820; https://doi.org/10.1088/1402-4896/ac6545

[9] Alsubaie, Munirah, Cheng Tang, Dimuthu Wijethunge, Dongchen Qi, Aijun Du, ACS Applied Electronic Materials 4, no. 7 (2022): 3240-3245; https://doi.org/10.1021/acsaelm.2c00476

[10] Xu, Yangsen, Hongning Kou, Shuohai Fang, Xianfen Wang, Lei Bi, Ceramics International 45, no. 17 (2019): 22383-22387; https://doi.org/10.1016/j.ceramint.2019.07.159

[11] Fang, Limin, Zhendong Hao, Liangliang Zhang, Hao Wu, Huajun Wu, Guohui Pan, Jiahua Zhang, Materials Research Bulletin 149 (2022): 111725; https://doi.org/10.1016/j.materresbull.2021.111725

[12] Li, T., R. J. Brook, B. Derby, Journal of the European Ceramic Society 19, no. 3 (1999): 399-405; https://doi.org/10.1016/S0955-2219(98)00178-2

[13] Roland, Christopher, Rashmi C. Desai, Physical Review B 42, no. 10 (1990): 6658; https://doi.org/10.1103/PhysRevB.42.6658

[14] Liu, Rongjuan, Zhiping Zhou, Yong Liu, Zhaopeng Liang, Yongqiang Ming, Yijing Nie, Tongfan Hao, Journal of Polymer Science Part B: Polymer Physics 57, no. 22 (2019): 1516-1526; https://doi.org/10.1002/polb.24897

[15] Zenga, Xiaoxing, Zhaodi Xuc, Xiaofeng Gonga, Yiqun Wanc, Ccatalyst 25: 28.

[17] Ni, Xiao-Sheng, Yue-Yu Zhang, Dao-Xin Yao, Yusheng Hou, Applied Physics Letters 122, no. 17 (2023); https://doi.org/10.1063/5.0145945

[18] Wang, Jingjing, Sajid Ur Rehman, Zeeshan Tariq, Xiaoming Zhang, Jun Zheng, Faheem K. Butt, Chuanbo Li, Solar Energy Materials and Solar Cells 230 (2021): 111258; https://doi.org/10.1016/j.solmat.2021.111258

[19] A.S. M. Aljaloud, A. F. Qasrawi, L. H. Kh. Alfhaid, Optical and Quantum Electronics (accepted)

[20] Sze, Simon M., Yiming Li, and Kwok K. Ng. Physics of semiconductor devices. John wiley & sons, 2021.

[21] Quan, Wenjing, Jia Shi, Hanyu Luo, Chao Fan, Wen Lv, Xinwei Chen, Min Zeng et al., ACS sensors 8, no. 1 (2023): 103-113; https://doi.org/10.1021/acssensors.2c01748

[22] Huang, Congcong, Xiaohai Ding, Xiaochen Ren, Xi Yu, Wenping Hu, Journal of Materials Chemistry C 10, no. 7 (2022): 2838-2844; https://doi.org/10.1039/D1TC05136A

[23] Qasrawi, Atef, Hazem Khanfar, Journal of the Arab American University 9, no. 1 (2023) 1-25.

[24] Qasrawi, A. F., Physica Scripta 89, no. 6 (2014): 065802; https://doi.org/10.1088/0031-8949/89/6/065802

[25] Singh, Mukhtiyar, Ramesh Kumar, Sunita Srivastava, Kumar Tankeshwar, Journal of Physics and Chemistry of Solids 172 (2023): 111083; https://doi.org/10.1016/j.jpcs.2022.111083

[26] Amato, Francesco, Christopher W. Peterson, Brian P. Degnan, Gregory D. Durgin. IEEE Journal of Radio Frequency Identification 2, no. 2 (2018): 93-103; https://doi.org/10.1109/JRFID.2018.2852498

[27] Cimbri, Davide, Jue Wang, Abdullah Al-Khalidi, Edward Wasige, IEEE Transactions on Terahertz Science and Technology 12, no. 3 (2022): 226-244; https://doi.org/10.1109/TTHZ.2022.3142965

[28] Dragoman, Mircea, Martino Aldrigo, Adrian Dinescu, Dan Vasilache, Sergiu Iordanescu, Daniela Dragoman, Nanomaterials 13, no. 3 (2023): 595; https://doi.org/10.3390/nano13030595

[29] Ramesh, S., Soon-Chien Lu, Journal of Molecular Liquids 177 (2013): 73-77; https://doi.org/10.1016/j.molliq.2012.09.018

[30] Qasrawi, Atef Fayez, Hadeel Mohammad Zyoud, Physica Status Solidi (a) 217, no. 22 (2020): 2000171; https://doi.org/10.1002/pssa.202000171

[31] Gupta, R. K., F. Yakuphanoglu, Solar Energy 86, no. 5 (2012): 1539-1545; https://doi.org/10.1016/j.solener.2012.02.015

[32] Dresselhaus, M., G. Dresselhaus, S. Cronin Filho, AGS: Solid State Properties From Bulk to Nano, (2017); https://doi.org/10.1007/978-3-662-55922-2

[33] Alfhaid, Latifah Hamad Khalid, Atef Fayez Qasrawi, Hazem K. Khanfar. Materials Today Communications 35 (2023): 106157; https://doi.org/10.1016/j.mtcomm.2023.106157

[34] Alfhaid, Latifah Hamad Khalid, Atef Fayez Qasrawi, Physica Scripta 97, no. 5 (2022): 055820; https://doi.org/10.1088/1402-4896/ac6545

[35] Kaya, A., S. Alialy, S. Demirezen, M. Balbaşı, S. Altındal Yerişkin, A. Aytimur, Ceramics International 42, no. 2 (2016): 3322-3329; https://doi.org/10.1016/j.ceramint.2015.10.126

[36] Kumar, Sumit, Amruta S. Dixit, Journal of Infrared, Millimeter, and Terahertz Waves 42, no. 9-10 (2021): 974-985; https://doi.org/10.1007/s10762-021-00799-2